Journal of Power Sources 195 (2010) 4667–4675

Contents lists available at ScienceDirect

Journal of Power Sources

journal homepage: www.elsevier.com/locate/jpowsour

Effect of firing temperature on the microstructure and performance of $PrBaCo_2O_{5+\delta}$ cathodes on $Sm_{0.2}Ce_{0.8}O_{1.9}$ electrolytes fabricated by spray deposition-firing processes

Dengjie Chen, Ran Ran, Zongping Shao*

State Key Laboratory of Materials-Oriented Chemical Engineering, College of Chemistry & Chemical Engineering, Nanjing University of Technology, No. 5 Xin Mofan Road, Gulou District, Nanjing 210009, PR China

ARTICLE INFO

Article history:
Received 12 January 2010
Received in revised form 28 January 2010
Accepted 29 January 2010
Available online 6 February 2010

Keywords:
Solid oxide fuel cells
Electrochemical impedance spectroscopy
Cathode
$PrBaCo_2O_{5+\delta}$
Layered perovskite

ABSTRACT

The effect of firing temperature on the microstructure and performance of $PrBaCo_2O_{5+\delta}$ cathodes on $Sm_{0.2}Ce_{0.8}O_{1.9}$ electrolytes fabricated by spray deposition-firing processes is systematically studied by various characterization techniques. The grain size, porosity and particle connection of the electrode as well as the physical contact between the $PrBaCo_2O_{5+\delta}$ and $Sm_{0.2}Ce_{0.8}O_{1.9}$ layers are influenced differently by the firing temperature. The area specific resistances (ASRs) of the various $PrBaCo_2O_{5+\delta}$ cathodes are measured by electrochemical impedance spectroscopy in both symmetrical two-electrode and three-electrode configurations. The lowest ASR and cathode overpotential are achieved at a firing temperature of 1000 °C. Two main oxygen reduction reaction processes are proposed according to the oxygen partial pressure dependence of the electrode ASR. The rate-determining step is transmitted from a charge-transfer process at low firing temperatures to a non-charge-transfer process at high firing temperatures. A fuel cell with the $PrBaCo_2O_{5+\delta}$ cathode fired at an optimal temperature of 1000 °C delivers the attractive peak power density of 835 mW cm^{-2} at 650 °C, while this density is much lower for other firing temperatures. This result suggests the firing temperature of $PrBaCo_2O_{5+\delta}$ electrodes should be carefully optimized for practical applications.

1. Introduction

Solid oxide fuel cells (SOFCs) are considered as promising alternative electric power generation devices to current fire power plants because of their high-energy conversion efficiency, environmental friendliness, and excellent fuel flexibility [1]. Additionally, it has been well recognized that the wide spread of this attractive technology can be greatly accelerated if its operation temperature is lowered from the conventional temperature of around 1000 °C to intermediate temperatures of 500–800 °C because of the multiple benefits including reduced fabrication and materials costs, prolonged lifetime, elegant sealing and versatile cell materials [2]. However, maintaining high cathodic performance and low electrolyte ohmic resistance at reduced operation temperature is a big challenge [3].

A typical SOFC cathode is composed of an electron-conducting $La_{0.8}Sr_{0.2}MnO_3$ (LSM) perovskite [4], over which the oxygen reduction reaction is strictly limited to the triple-phase boundary (TPB) where the electrode, the electrolyte and the gas phase meet [5]. With a drop in operation temperature, the cathodic polarization resistance increases so sharply that LSM is no longer applicable at intermediate temperatures. Currently, there is considerable research activity on the potential of novel mixed ionic and electronic conductors as cathode materials of intermediate-temperature solid oxide fuel cells (IT-SOFCs) [6–9]. The mixed conductivity of such materials greatly extends the reaction sites, and consequently, these materials are expected to provide much higher electrode activity for oxygen reduction than LSM at reduced temperatures. Indeed, some materials, such as $La_xSr_{1-x}Co_yFe_{1-y}O_{3-\delta}$ [10–14], $Sm_xSr_{1-x}CoO_{3-\delta}$ [15–17] and $Ba_xSr_{1-x}Co_yFe_{1-y}O_{3-\delta}$ [18–22] perovskites, have been reported to have high electrochemical activity at temperatures as low as 600 °C. Recently, several research teams have reported the potential application of cation-ordered double-perovskite $LnBaCo_2O_{5+\delta}$ (Ln = Gd, Pr, Y, La, etc.) as cathodes of IT-SOFCs [23–35]. Based on a symmetric cell test, we have previously demonstrated that acceptable area specific resistance (ASR) can be achieved for $PrBaCo_2O_{5+\delta}$ (PrBC) cathodes at intermediate temperature [33].

With the further investigation into these cathode materials, however, some discrepancies appeared in the literature. The reported ASR of electrodes composed of the same material and tested under similar conditions could vary by several orders of

* Corresponding author. Tel.: +86 25 83172256; fax: +86 25 83172256.
E-mail address: shaozp@njut.edu.cn (Z. Shao).

0378-7753/$ – see front matter © 2010 Elsevier B.V. All rights reserved.
doi:10.1016/j.jpowsour.2010.01.082

magnitude; for example, the reported ASRs at 600 °C in air were in the wide range of 1.9–5.5 Ω cm^2 for $Sm_{0.5}Sr_{0.5}CoO_{3-\delta}$ [15,17] and 0.071–0.51 Ω cm^2 for $Ba_{0.5}Sr_{0.5}Co_{0.8}Fe_{0.2}O_{3-\delta}$ [18,36].

It is well known that in addition to the intrinsic properties of cathode materials, which depend on the material composition and lattice structure, their electrode performance is also closely related to their microstructure [11,37–39] and to the interfacial phase reaction between the electrode and electrolyte [40]. The discrepancy in electrode performance of the cathodes composed of the same material reported by different authors may be a result of their different electrode microstructures and/or different interfacial reaction behavior.

To fabricate a cathode layer on an electrolyte surface, crystallized cathode material is first prepared by various methods, such as solid-state reaction, sol–gel synthesis and many other advanced techniques, and then the cathode material is deposited onto the electrolyte surface and co-fired with the electrolyte layer at a high temperature. Previous works have shown that the ASR of many cathodes strongly depends on the firing temperature [11,37]. For example, Leng et al. reported that the electrode polarization resistance of $La_{0.6}Sr_{0.4}Co_{0.2}Fe_{0.8}O_{3-\delta}$ electrodes fired at 975 °C is much lower than that of electrodes fired at other temperatures [11]. A detailed investigation into the effect of firing temperature on electrode performance would be helpful in optimizing the cell performance.

In the present study, PrBC was applied as the cathode for a SOFC with $Sm_{0.2}Ce_{0.8}O_{1.9}$ (SDC) electrolyte. The influence of firing temperature on the microstructure and performance of a PrBC cathode was systematically studied and explained. The optimized firing temperature was developed.

2. Experimental

2.1. Powder synthesis and cell fabrication

Both PrBC and SDC oxide powders were prepared by a combined EDTA-citrate complexing sol–gel process. $Sm(NO_3)_3{\cdot}6H_2O$ (A.R., Aladdin Reagent Co., Ltd., Shanghai, China) and $Ce(NO_3)_3{\cdot}6H_2O$ (A.R., Sinopharm Chemical Reagent Co., Ltd., Shanghai, China) were applied as the raw materials to synthesize SDC. The synthesis of PrBC, for example, was performed as follows. Stoichiometric amounts of $Pr(NO_3)_3{\cdot}6H_2O$ (A.R., Aladdin Reagent Co., Ltd., Shanghai, China), $Ba(NO_3)_2$ (A.R., Sinopharm Chemical Reagent Co., Ltd., Shanghai, China) and $Co(NO_3)_2{\cdot}6H_2O$ (A.R., Sinopharm Chemical Reagent Co., Ltd., Shanghai, China), were prepared into a mixed solution, and then EDTA–$NH_3{\cdot}H_2O$ and citric acid, serving as complexing agents, were added in sequence at a mole ratio for total metal ions to EDTA to citric acid of 1:1:2 under heating and stirring. After vaporizing the water from the solution via heating, a transparent gel was obtained. The gel was pre-fired at 250 °C to form a black solid precursor, which was subsequently calcinated at 950 °C for 5 h in an air atmosphere to remove the carbon residue and to form the desired $PrBaCo_2O_{5+\delta}$ phase.

To measure the electrode performance, both a symmetric cell and a three-electrode configurations were adopted and tried, as shown in Fig. 1. The SDC electrolyte pellets prepared for symmetric two-electrode and three-electrode cells were fabricated by dry pressing SDC powder (particle size, 22.9 nm) into disk-shaped pellets using stainless steel dies under hydraulic pressure of 200 MPa, followed by sintering at 1450 °C for 5 h in air. The resulting dense pellets (relative density, 95.8%) have diameters of approximately 12 and 16 mm, respectively, for the two-electrode symmetric cells and the three-electrode cells. To prepare the electrode layers of symmetric cells, PrBC oxide was well dispersed in a mixed solution of ethylene glycol, ethanol and isopropyl alcohol using a high-energy ball miller (Fritsch, Pulverisette 6) at the rotational speed of 400 rpm for 0.5 h; it was then symmetrically deposited onto both surfaces of the electrolyte by air-driven spray, followed by firing at 900–1100 °C in air for 2 h. To prepare a three-electrode cell, PrBC slurry was painted on one side of the SDC electrolyte to form a round electrode with an area of 0.26 cm^2, which acts as a working electrode (WE), followed by firing at 900–1100 °C in air for 2 h. A Pt electrode, with the same shape and position as the WE, was painted on the other side of the SDC electrolyte pellet to act as a counter electrode (CE) followed by firing at 900 °C in air for 30 min. A silver (DAD-87, Shanghai Research Institute of Synthetic Resins, Shanghai, China) electrode was ringed around the counter electrode to act as a reference electrode (RE). The gap between the counter and the reference electrode was about 4 mm to prevent systematic errors in electrochemical measurements.

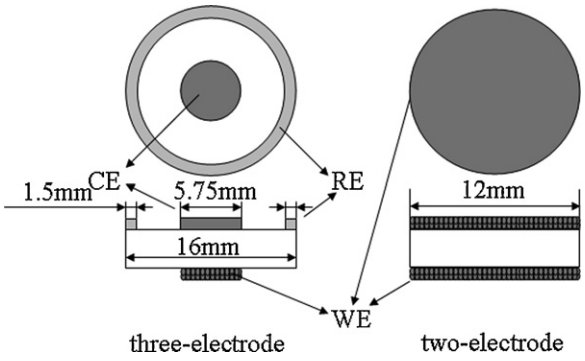

Fig. 1. The schematic diagram of the symmetrical two-electrode and three-electrode structures for impedance and overpotential measurements.

Anode-supported thin-film SDC electrolyte dual-layer cells were prepared via dual dry pressing. Well mixed powders containing 60 wt% NiO (A.R., particle size, ~8 μm, Shudu Nano-Science Development Co., Ltd., Chengdu, China) and 40 wt% SDC were applied as anode starting materials, which were pressed into a green pellet using a 15-mm stainless steel die. The proper amount of SDC powder was dispersed homogeneously over the open surface of the green anode pellet inside the die and pressed again to form a dual-layer pellet. These green cells were then densified at 1450 °C for 5 h in an air atmosphere. The PrBC slurry was then spray-deposited over the electrolyte surface, followed by firing at 900–1100 °C in air for 2 h to form complete cells with an effective area of 0.48 cm^2 of the porous cathode layer. The three-layered pellets NiO + SDC|SDC|PrBC were then used for *I–V* characterization.

2.2. Electrochemical characterization

Electrochemical impedance spectroscopy (EIS) was conducted using symmetric two-electrode and three-electrode configurations. Both the electrode surfaces of the symmetric cells and WE-surface of the three-electrode cells were painted with a thin layer of silver to act as current collectors. The cells were then loaded into a quartz tube reactor with controllable atmosphere. The ASR of the electrode was determined from its EIS using a Solartron 1260 Frequency Response Analyzer in combination with a Solartron 1287 potentiostat. The frequency used for EIS measurements ranged from 10^{-1} to 10^5 Hz, and the signal amplitude was 10 mV with no applied dc bias. The overall impedance data were collected with the ZPlot 2.9c software program and fitted by a complex non-linear least squares (CNLS) fitting program using the ZView 2.9 software program. The oxygen partial pressure of the atmosphere was varied between 0.04 and 1 atm by mixing O_2 with N_2 using mass flow controllers.

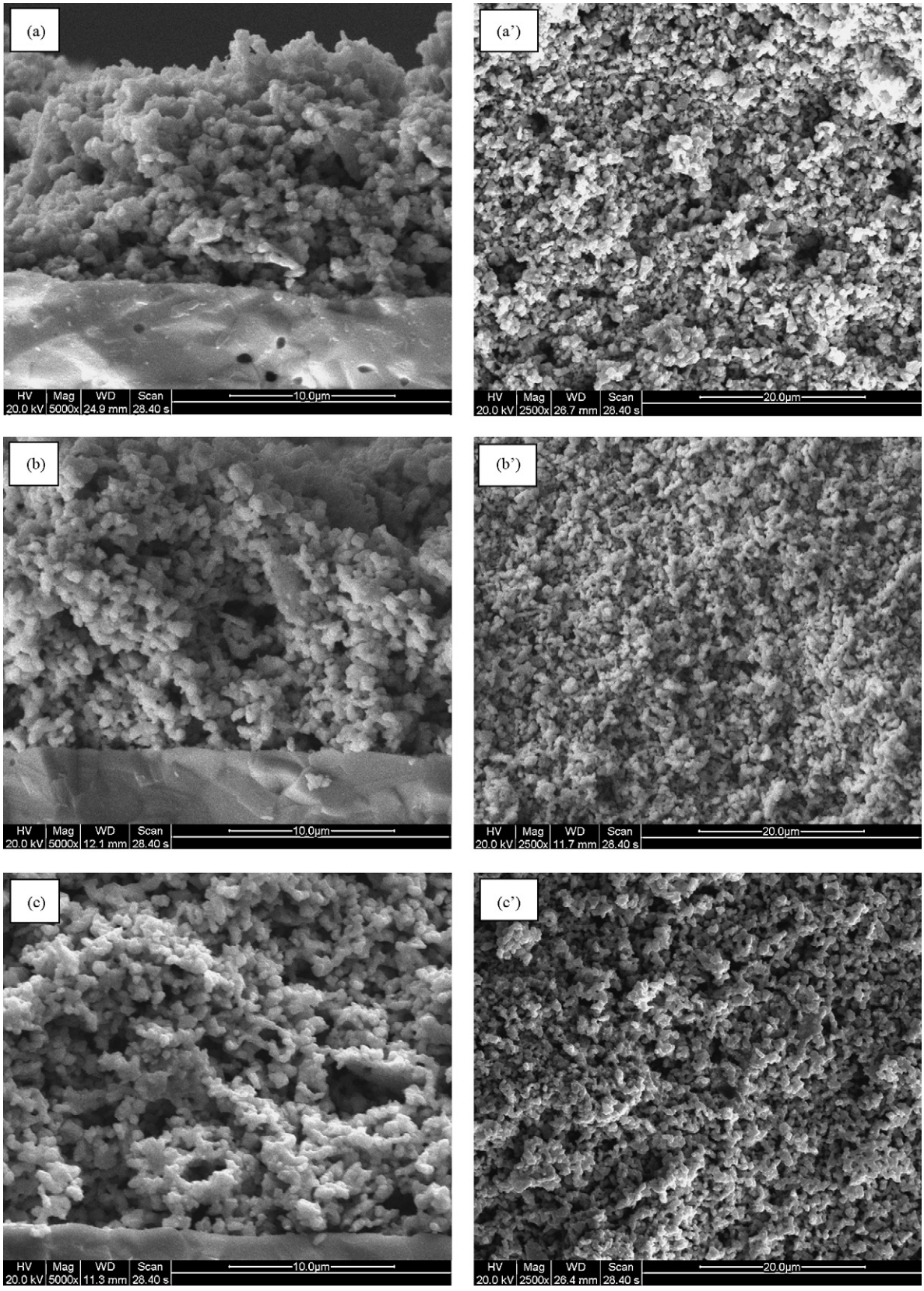

Fig. 2. SEM images of the symmetrical two-electrode cells from both the cross-sectional and top views, with the cathode fired at the temperatures of (a, a′) 900 °C, (b, b′) 950 °C, (c, c′) 1000 °C, (d, d′) 1050 °C, and (e, e′) 1100 °C.

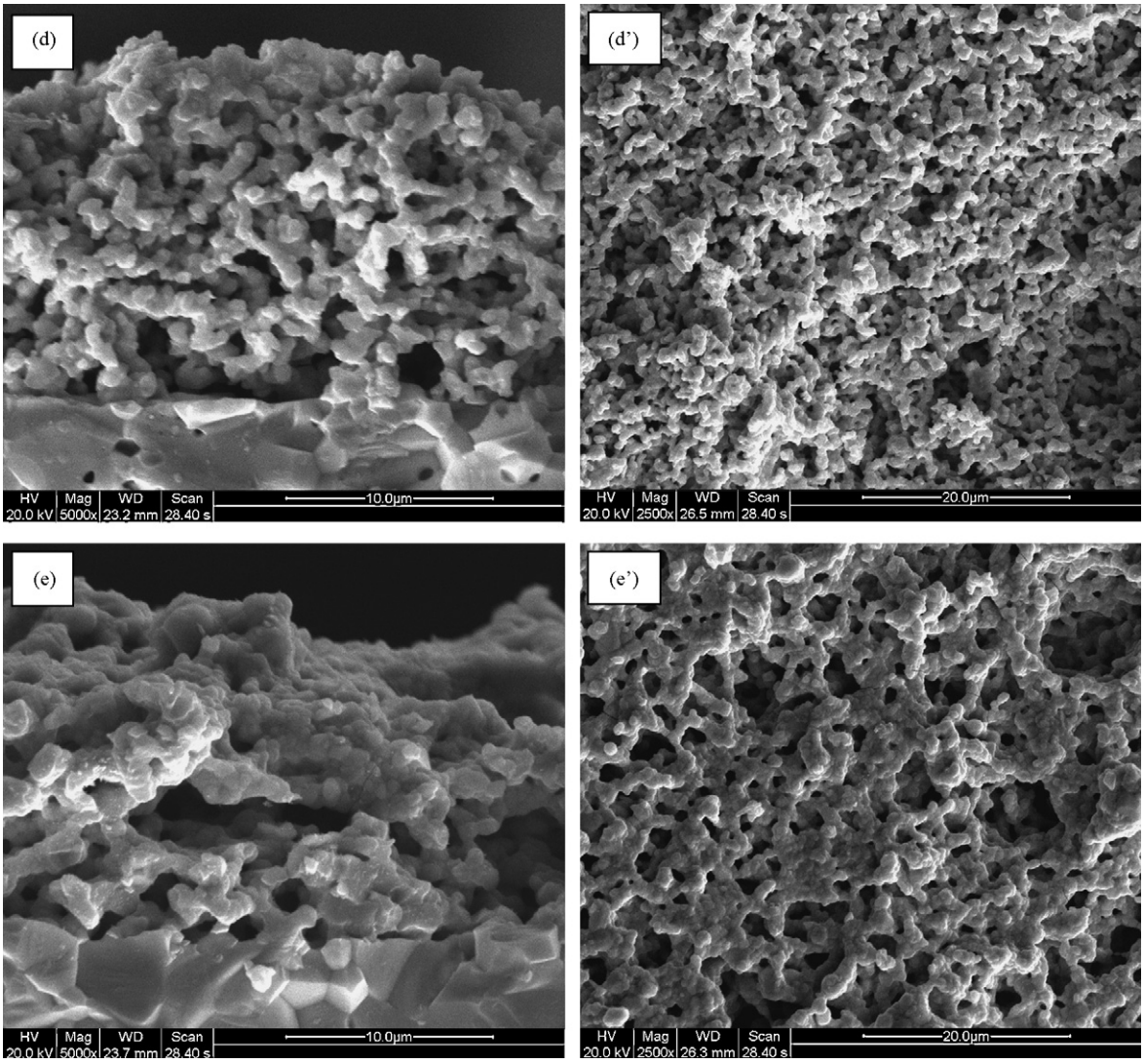

Fig. 2. (*Continued*).

The cathodic overpotential was measured using a Solartron 1287 potentiostat/galvanostat, which was operated via the Corrware 2.9c software. The polarization current density was varied from 0 to 1000 mA cm^{-2} in 10 mA cm^{-2} intervals. The IR drop, originating from the electrolyte and lead/contact resistances, was compensated to establish the IR-free I/E polarization curves.

The performance of the cathode fired at different temperatures was also evaluated in complete cells in an in-lab constructed SOFC test station. The cell was sealed onto the top of a quartz tube with silver to act as a fuel cell reactor, which was put into a vertical split tube furnace. The cathode side and anode side were fed with ambient air and humidified hydrogen at a flow rate of 80 ml min^{-1}, respectively. A thermocouple was inserted near the cathode surface for the temperature monitoring. A digital sourcemeter (Keithley 2420) was used for I–V polarization testing based on a four-terminal configuration.

3. Results and discussion

3.1. Microstructure

To fabricate PrBC cathodes on the SDC electrolytes, PrBC in suspension form was first spray-deposited onto the surface of a SDC disk, followed by high-temperature firing. The firing temperature may affect the microstructure of PrBC electrode by influencing its surface area, porosity, particle connection, and physical contact with the electrolyte layer; it may also induce an interfacial reaction between the SDC electrolyte and PrBC electrode layers. An insufficient porosity may create a serious concentration polarization, especially at high polarization current density. On the one hand, poor connection between electrode particles and/or poor physical contact between the electrolyte and electrode layers may hinder the charge transfer from particle to particle in the electrode, and/or from the electrode to the electrolyte; as a result, a large electrode polarization resistance is expected. On the other hand, the reduction in surface area because of sintering decreases the active sites for oxygen adsorption, dissociation and surface diffusion; as a result, an increase in electrode polarization resistance is expected. In addition, the phase reaction could create an interfacial phase, which may block the oxygen diffusion and lead to a sharp increase in the cell resistance.

The microstructure of the PrBC electrodes fired at different temperatures was then examined by SEM observation. Fig. 2 shows the micrographs of the PrBC cathodes, both from the surface and cross-sectional views. For all firing temperatures, the electrodes show porous structures but with different levels of porosity, which are given in Table 1. As a whole, a decrease in porosity with increasing firing temperature was observed. In particular, the electrode fired

Table 1
The porosity values of $PrBaCo_2O_{5+\delta}$ cathodes fired from 900 to 1100 °C.

Firing temperature (°C)	900	950	1000	1050	1100
Porosity (%)	41.8	37.5	35.9	27.3	18.1

at 1100 °C was seriously sintered both at the surface and in the interior. The electrodes fired at 900 and 950 °C have high porosity and fine particle size; however, they also show relatively poor particle connections. With the increase of firing temperature to 1000 °C, the particle connection of the electrode improved noticeably, while the grain size increased only slightly. The average grain sizes are ~0.65, 0.72 and 0.75 μm for the electrodes fired at 900, 950 and 1000 °C, respectively. With further increases in firing temperature, however, an obvious increase in grain size with the temperature was also observed. The electrode fired at 1050 and 1100 °C had average grain sizes of ~1.64 and 2.62 μm, respectively, which are ~2.5 and 4 times that of the electrode fired at 900 °C.

3.2. Electrochemical performance

The electrochemical performance of the various electrodes was first investigated by EIS in symmetric cell configuration. The typical EIS in the Nyquist plots of the various cells from firing at different temperatures are shown in Fig. 3. All the EIS include a high-frequency induction tail and a depressed arc. Since there was no serious phase reaction between PrBC and SDC within the whole temperature range investigated, of 900–1100 °C [33], the ohmic resistance of the cell is not discussed in the following section. It was found that the corresponding frequency point, such as 100 Hz, shifted to the left intersection of the real axis of EIS with increased cathode firing temperature, implying that the rate-determining step of oxygen reduction reaction kinetics likely changed with the increase of firing temperature.

It is well known that the oxygen reaction over a mixed conducting electrode is complex, which may include several sub-steps,

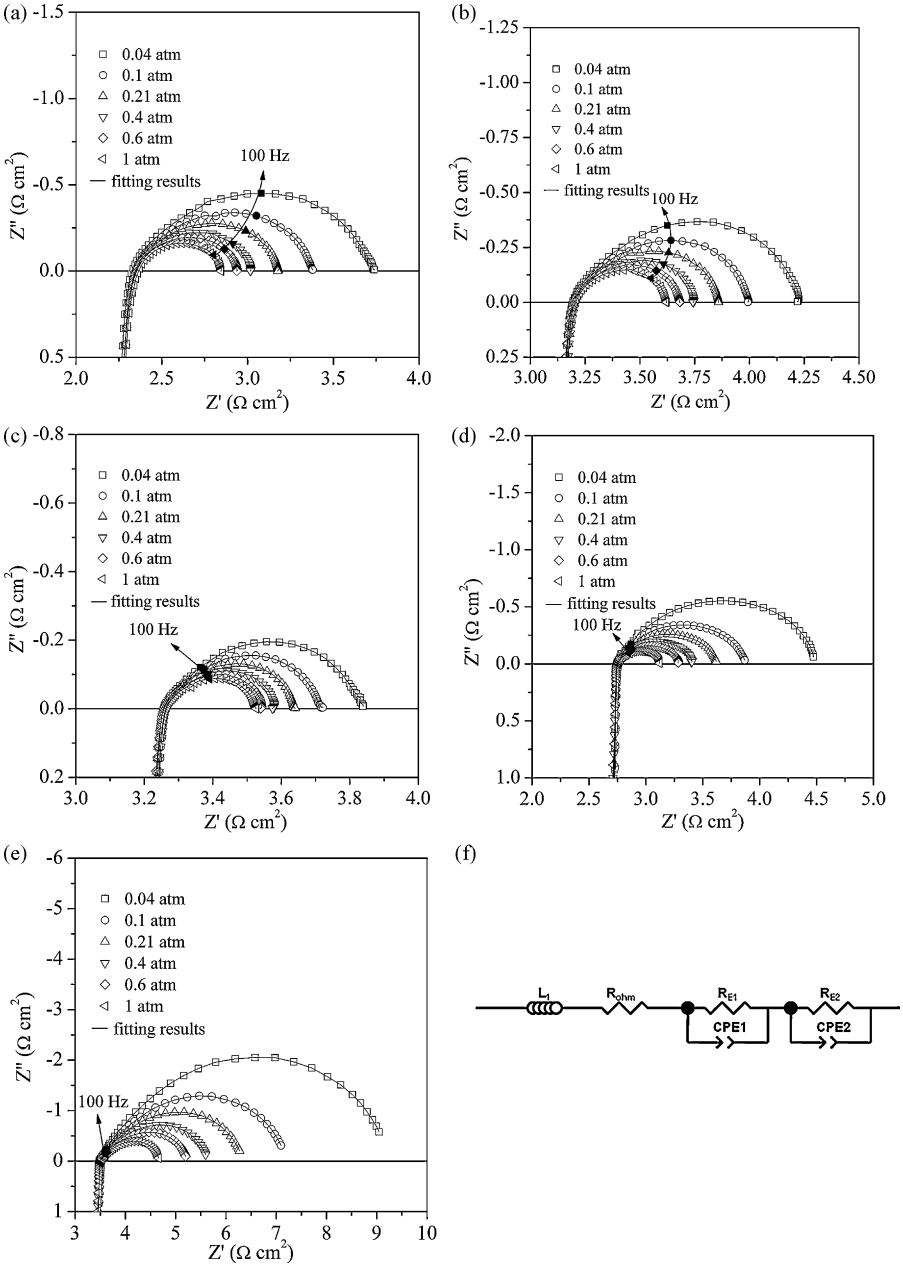

Fig. 3. Impedance spectroscopy for symmetrical two-electrode cells in Nyquist plots measured at open circuit voltage and tested at 600 °C in oxygen partial pressure from 0.04 to 1 atm, with cathode fired at (a) 900 °C; (b) 950 °C; (c) 1000 °C; (d) 1050 °C; and (e) 1100 °C. The equivalent circuits adopted for fitting the EIS data is shown in (f).

such as surface oxygen diffusion, adsorption, dissociation, and charge transfers (both oxygen ions and electrons) [41–43]. The firing temperature has different impacts on the above processes; consequently a change in the rate-determining step could happen with the change of firing temperature. To get more insight into the effect of firing temperature on the performance of PrBC electrode, EIS of the symmetric cells at different oxygen partial pressures were measured. Fig. 3a–e shows the EIS for the various PrBC cathodes in Nyquist plots, tested at 600 °C in atmosphere with oxygen partial pressure varied from 0.04 to 1 atm. The data were fitted to an equivalent circuit shown in Fig. 3f. Here (R_{E1}-CPE1) and (R_{E2}-CPE2) representthe processes at high and low frequency, respectively. The constant phase element (CPE) represents a non-ideal capacitor, and the associated CPE-P parameter indicates the similarity of the CPE to a true capacitor, for which CPE-P = 1. The symbols in Fig. 3a–e represent the measured data, while the solid lines are fitted curves. Good agreement between the fitted curves and the observed impedance data was observed. This implies that the equivalent circuit is a reasonable approximation for fitting the experimental data.

It is well accepted that different processes for oxygen reduction reaction over mixed ionic and electronic conducting electrodes have different levels of dependence on the oxygen partial pressure [43,44]. The most commonly used parameter to determine the step in the oxygen reduction process is m, which indicates the relationship between the polarization resistance and oxygen partial pressure, expressed as $\ln(1/R) = m\ln(pO_2)$. The m values give information about the type of oxygen species involved in the oxygen reduction reaction, as listed in Table 2. Typically, m values between 0.5 and 1 indicate non-charge-transfer processes, which include oxygen diffusion at the gas–cathode interface, adsorption–desorption of oxygen, and the surface diffusion of adsorbed oxygen species. The value 0.25 should be observed for a charge-transfer process [43,44], which could happen at the air–electrode interface and electrode–electrode interface. The value 0 indicates the ion charge transfer from the electrode to electrolyte [40]. It is often difficult to separate the two processes (m = 0.25 and m = 0) in the EIS because they typically have similar characteristic frequency [45]. Fig. 4 shows oxygen partial pressure dependence of the fitted R_{E1} and R_{E2}. It can be observed that

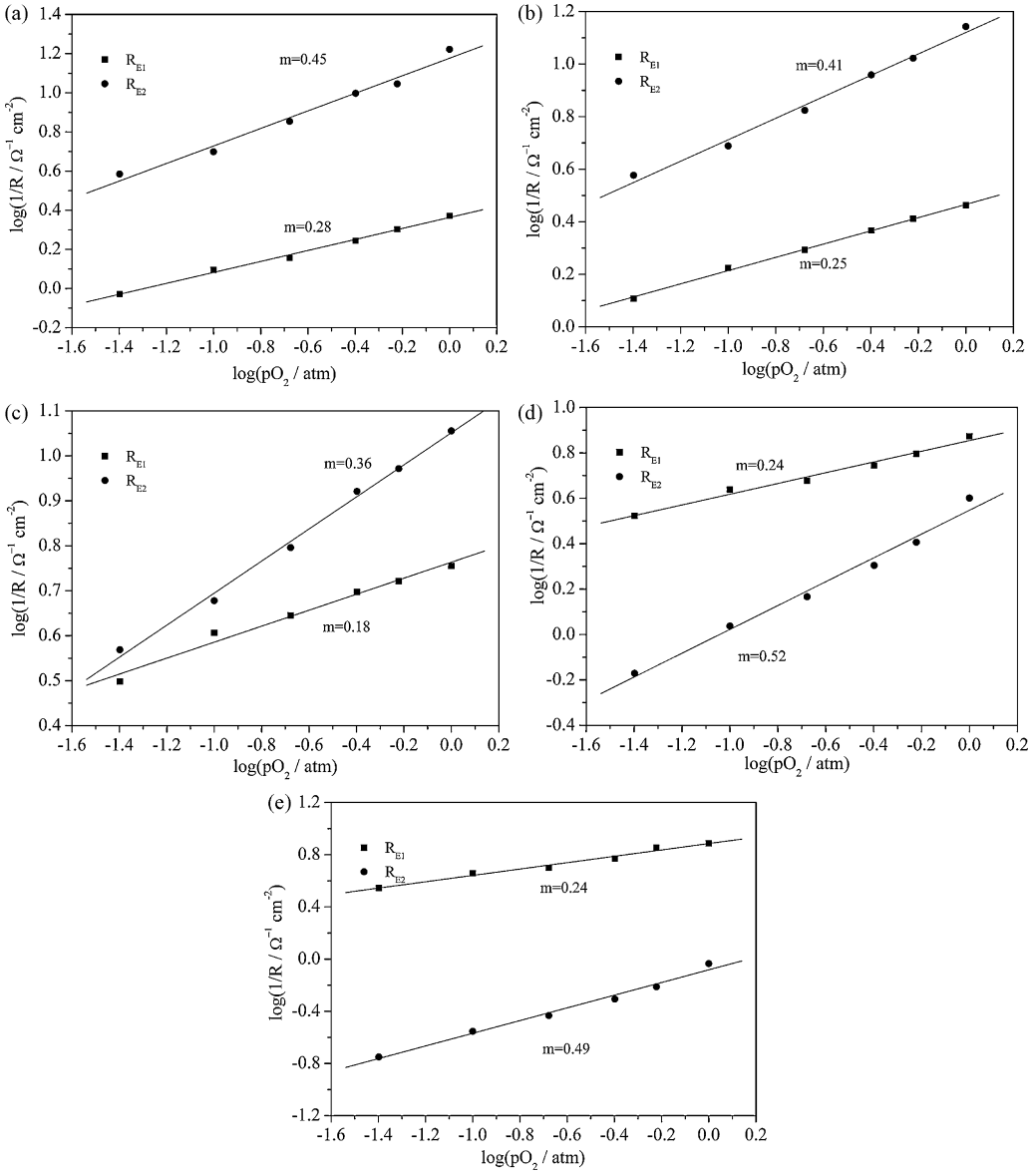

Fig. 4. Dependence on the oxygen partial pressure of the fitted R_{E1} and R_{E2} with cathode fired at (a) 900 °C; (b) 950 °C; (c) 1000 °C; (d) 1050 °C; and (e) 1100 °C.

Table 2
Oxygen reduction reaction steps and the values of m in $\ln(1/R) = m\ln(pO_2)$.

Reaction steps	m
$O_{2,gas} \Leftrightarrow O_{2,ads}$	1
$O_{2,ads} \Leftrightarrow 2O_{O,ads}$	0.5
$O_{ads} \Leftrightarrow O_{ads,erz}$	0.5
$O_{ads,erz} + V^{\bullet\bullet}_{O,electrode} + 2e' \Leftrightarrow O^{\times}_{O,electrode}$	0.25
$O^{\times}_{O,electrode} \Leftrightarrow O^{\times}_{O,electrode}$	0.25
$O^{\times}_{O,electrode} \Leftrightarrow O^{\times}_{O,electrolyte}$	0

erz: effective reaction zone.

$\ln(1/R_{E1})$ had a $\ln(pO_2)$ dependent slope of 0.18–0.28, which implies that this process is likely related to the charge-transfer process. On the other hand, $\ln(1/R_{E2})$ had a $\ln(pO_2)$ dependent slope of 0.36–0.52, indicating the non-charge-transfer process. It should be pointed out that the concentration polarization arc did not appear under all conditions. This may due to the porosity of the PrBC cathode fired at 900–1100 °C is sufficient for free gas diffusion ($m = 1$) under conditions without a polarization current.

Fig. 5 presents the fitted R_{E1} and R_{E2} (derived from Fig. 3) of the PrBC cathode as a function of the firing temperature, measured in an air atmosphere. As a whole, R_{E1} decreased while R_{E2} increased with increasing temperature. R_{E1} decreased noticeably with firing temperature between 900 and 1000 °C, after which the decrement became much smaller with further increases in firing temperature. As to R_{E2}, which is related to the non-charge-transfer process, it increased only slightly with firing temperature between 900 and 1000 °C, while with further increases in firing temperature a sharp increase in R_{E2} was then observed. The SEM results, shown in Fig. 2, can now be well explained as follows. At the temperature range of 900–1000 °C, the increase in firing temperature did not have a significant impact on the grain size (surface area) of the electrode, while it led to an obvious improvement of the electrode particle connection; as a result, the surface processes were not seriously affected but the charge-transfer process was greatly improved. At firing temperatures higher than 1000 °C, the particle connection was well developed, so that the further increase in firing temperature did not lead to an obvious change in R_{E1}; however, significant sintering of the electrode appeared, which led to an obvious decrease in the surface area, and consequently the non-charge-transfer surface processes were greatly impaired. Table 3 summarizes the values of R_{E1} and R_{E2} (derived from Fig. 3) at various oxygen partial pressures. The same tendency was observed at all other oxygen partial pressures. The optimal firing temperature that leads to the minimum value of the sum of R_{E1} and R_{E2} was found to be around 1000 °C.

Cathodic overpotential is an important factor representing electrode performance. Three-electrode cells were fabricated to evaluate the performance of the various electrodes under current polarization conditions. It is well known that the accuracy of three-electrode test is strongly dependent on the preparation technique. To ensure the high reliability of the data, the work electrode and the counter electrode should be as symmetric as possible, while the reference electrode should be as far from the electrode as possible. To ensure the high reliability of the three-electrode electrochemical test in the current study, the cell was first tested without DC polarization, and the data obtained were compared with those obtained from two-electrode symmetric cell tests. ASR values from the symmetric two-electrode and three-electrode cells for a cathode fired at different temperatures tested at 600 °C in air, for example, are plotted in Fig. 6. A line with the slope of 1 was drawn for reference. Good agreement in polarization resistance is obtained in both configurations, suggesting the high reliability of the three-electrode cells in the current study.

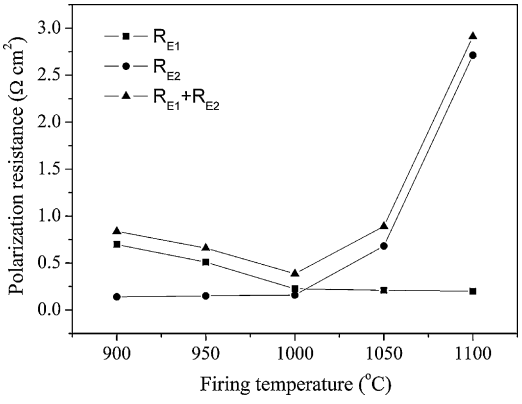

Fig. 5. Typical plots of the firing temperature dependence of R_{E1}, R_{E2} and $R_{E1} + R_{E2}$, which was derived from the fitting results of Fig. 3 (tested at 600 °C, air atmosphere).

Table 3
The fitting parameters R_{E1} and R_{E2} (derived from Fig. 3) as functions of oxygen partial pressure and cathode firing temperature for $PrBaCo_2O_{5+\delta}$/SDC/$PrBaCo_2O_{5+\delta}$ under zero *dc* bias conditions.

	T (°C)				
	900	950	1000	1050	1100
pO_2: 0.04 atm					
R_{E1} (Ω cm²)	1.068	0.782	0.318	0.300	0.285
R_{E2} (Ω cm²)	0.260	0.265	0.270	1.483	5.621
$(R_{E1} + R_{E2})$ (Ω cm²)	1.328	1.047	0.588	1.783	5.906
pO_2: 0.1 atm					
R_{E1} (Ω cm²)	0.804	0.597	0.247	0.230	0.220
R_{E2} (Ω cm²)	0.200	0.205	0.210	0.918	3.580
$(R_{E1} + R_{E2})$ (Ω cm²)	1.004	0.802	0.457	1.148	3.800
pO_2: 0.21 atm					
R_{E1} (Ω cm²)	0.698	0.509	0.226	0.210	0.200
R_{E2} (Ω cm²)	0.140	0.150	0.160	0.681	2.712
$(R_{E1} + R_{E2})$ (Ω cm²)	0.838	0.659	0.386	0.891	2.912
pO_2: 0.4 atm					
R_{E1} (Ω cm²)	0.570	0.430	0.201	0.180	0.170
R_{E2} (Ω cm²)	0.101	0.110	0.120	0.496	2.024
$(R_{E1} + R_{E2})$ (Ω cm²)	0.671	0.540	0.321	0.676	2.194
pO_2: 0.6 atm					
R_{E1} (Ω cm²)	0.498	0.388	0.190	0.160	0.140
R_{E2} (Ω cm²)	0.090	0.095	0.107	0.392	1.630
$(R_{E1} + R_{E2})$ (Ω cm²)	0.588	0.483	0.297	0.552	1.770
pO_2: 1 atm					
R_{E1} (Ω cm²)	0.425	0.345	0.176	0.134	0.130
R_{E2} (Ω cm²)	0.060	0.072	0.088	0.251	1.082
$(R_{E1} + R_{E2})$ (Ω cm²)	0.485	0.417	0.264	0.385	1.212

To evaluate the performance of the various electrodes under current polarization, a current was then introduced between the working electrode and the counter electrode. The IR-corrected Tafel plots for the PrBC cathode, as a function of cathode firing temperature tested at 600 °C in air, are shown in Fig. 7. At the overpotential of −0.15 V, the cathode current density was found to be around 135, 150, 205, 135 and 100 mA cm^{-2} in air at cathode firing temperatures of 900, 950, 1000, 1050 and 1100 °C, respectively. Although the graph indicates that three-electrode cells underestimate overpotential within several to 10%, the lowest cathode overpotential is achieved for the cathode fired at 1000 °C, in accordance with the EIS results.

3.3. Single cell performance

Ni + SDC anode-supported thin-film SDC electrolyte fuel cells were fabricated to evaluate the performance of the PrBC electrode under real fuel cell operation conditions. Fig. 8 shows the *I–V* and *I–P* curves of the cells with PrBC electrode being fired at various tem-

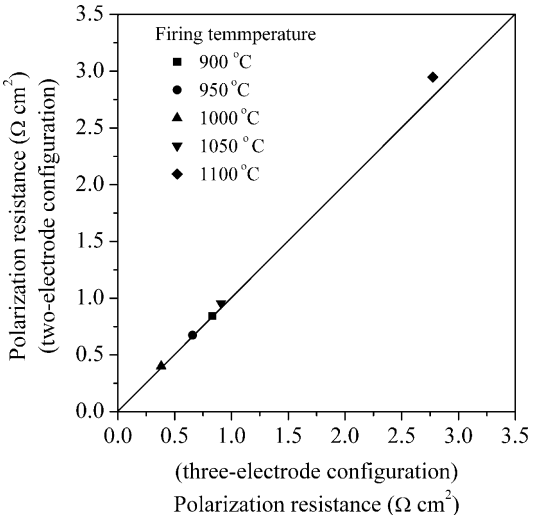

Fig. 6. A comparison of the electrode area specific resistances measured in the symmetric two-electrode and three-electrode configurations. The test was conducted at 600 °C in air at open circuit voltage.

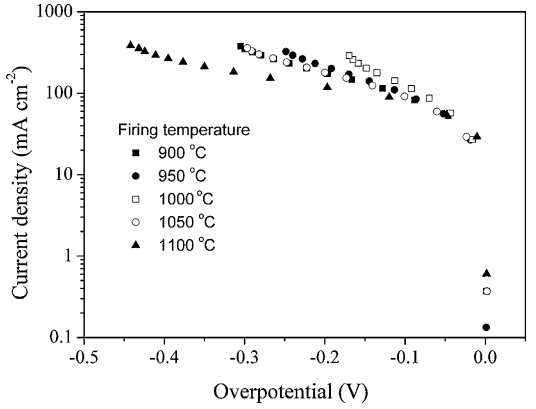

Fig. 7. The IR-corrected Tafel plots for the PrBC cathode fired at different temperatures and tested at 600 °C in air.

peratures. The test was conducted at 650 °C with ambient air as the cathode atmosphere and humidified hydrogen with 80 ml min^{-1} as the anode fuel. Since the anodes and electrolyte were fabricated following an identical procedure, the anode and electrolyte resistances of the various cells were reasonably assumed to be the same, so the main contribution to the difference in cell performance is from the PrBC cathode. A maximum peak power density

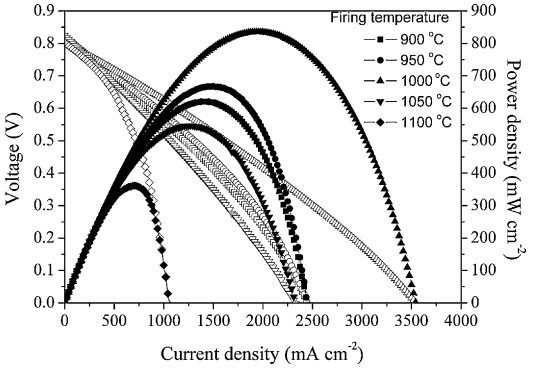

Fig. 8. The *I–V* and *I–P* curves of the cells with cathodes fired at different temperatures at 650 °C, with ambient air applied as the cathode atmosphere and humidified hydrogen with 80 ml min^{-1} as the anode fuel.

of 835 mW cm^{-2} was achieved from the cell with the PrBC cathode fired at 1000 °C, which was much higher than those of the cells with the cathode fired at other temperatures, where densities of 621, 667, 546 and 360 mW cm^{-2} at firing temperatures of 900, 950, 1050 and 1100 °C, respectively. It was observed that the dependence of the cell voltage on the current density of cells is basically a straight line except for the cathode fired at 1100 °C. This suggests that the porosity of the cathode fired at 900–1000 °C is sufficient for free gas diffusion. As to the PrBC cathode fired at 1100 °C, due to the significant sintering during the high-temperature firing, noticeable concentration polarization likely occurred at the high current density.

4. Conclusions

The firing temperature has significant effects on the microstructure and, consequently, the electrode performance of PrBC cathode. It affects the surface area, porosity, particle size, and particle connection of PrBC electrodes differently. An increase in firing temperature led to an obvious increase in particle connection of the electrode between 900 and 1000 °C, while the particle size was not significantly affected within this temperature range. With further increases in firing temperature, however, the particle size increased appreciably. The porosity of the electrode decreased monotonically with increasing firing temperature; however, only the electrode fired at 1100 °C showed significant sintering. Within the full temperature range of 900–1100 °C, there was no obvious phase reaction between PrBC and SDC electrolyte based on the powder reaction test. The electrode performance was determined by the complicated effects of the firing temperature on the microstructure of the PrBC electrode. The cathode firing temperature should be carefully optimized to get maximum power output by applying the PrBC cathode. As a whole, an increase in the electrode polarization resistance associated with non-charge-transfer processes and a decrease in the electrode polarization resistance associated with charge-transfer processes was observed with increasing firing temperature. The optimal firing temperature is that at which the overall electrode polarization resistance reaches minimum, which was found to be around 1000 °C for PrBC electrodes in this study. A cell with PrBC electrodes fired at 1000 °C delivered a peak power density of 835 mW cm^{-2} at 650 °C, which is more than double that of a similar cell with PrBC electrode fired at 1100 °C.

Acknowledgements

This work was supported by the National Natural Science Foundation of China under Contract Nos. 20676061 and 20703024, by the National 863 Program under Contract No. 2007AA05Z133 and by the National Basic Research Program of China under Contract No. 2007CB209704.

References

[1] B.C.H. Steele, A. Heinzel, Nature 414 (2001) 345–352.
[2] N.P. Brandon, S. Skinner, B.C.H. Steele, Annu. Rev. Mater. Res. 33 (2003) 183–213.
[3] J. Fleig, F.S. Baumann, V. Brichzin, H.-R. Kim, J. Jamnik, G. Cristiani, H.-U. Habermeier, J. Maier, Fuel Cells 6 (2006) 284–292.
[4] N.Q. Minh, J. Am. Ceram. Soc. 76 (1993) 563–588.
[5] M. Mogensen, S. Skaarup, Solid State Ionics 86–88 (1996) 1151–1160.
[6] J.M. Ralph, C. Rossignol, R. Kumar, J. Electrochem. Soc. 150 (2003) A1518–A1522.
[7] K.T. Lee, A. Manthiram, J. Electrochem. Soc. 153 (2006) A794–A798.
[8] K.K. Hansen, K.V. Hansen, Solid State Ionics 178 (2007) 1379–1384.
[9] W. Zhou, Z.P. Shao, R. Ran, R. Cai, Electrochem. Commun. 10 (2008) 1647–1651.
[10] Y.J. Leng, S.H. Chan, S.P. Jiang, K.A. Khor, Solid State Ionics 170 (2004) 9–15.
[11] Y.J. Leng, S.H. Chan, Q.L. Liu, Int. J. Hydrogen Energy 33 (2008) 3808–3817.
[12] E.P. Murray, M.J. Sever, S.A. Barnett, Solid State Ionics 148 (2002) 27–34.
[13] W.G. Wang, M. Mogensen, Solid State Ionics 176 (2005) 457–462.

[14] S. Bebelis, N. Kotsionopoulos, A. Mai, F. Tietz, J. Appl. Electrochem. 37 (2007) 15–20.
[15] J. Peña-Martínez, D. Marrero-López, D. Pérez-Coll, J.C. Ruiz-Morales, P. Núñez, Electrochim. Acta 52 (2007) 2950–2958.
[16] X.G. Zhang, M. Robertson, S. Yick, C. Deces-Petit, E. Styles, W. Qu, Y.S. Xie, R. Hui, J. Roller, O. Kesler, R. Maric, D. Ghosh, J. Power Sources 160 (2006) 1211–1216.
[17] H. Lv, Y.J. Wu, B. Huang, B.Y. Zhao, K.A. Hu, Solid State Ionics 177 (2006) 901–906.
[18] Z.P. Shao, S.M. Haile, Nature 431 (2004) 170–173.
[19] J. Peña-Martínez, D. Marrero-López, J.C. Ruiz-Morales, B.E. Buergler, P. Núñez, L.J. Gauckler, Solid State Ionics 177 (2006) 2143–2147.
[20] Z.H. Chen, R. Ran, W. Zhou, Z.P. Shao, S.M. Liu, Electrochim. Acta 52 (2007) 7343–7351.
[21] W. Zhou, R. Ran, Z.P. Shao, W. Zhuang, J. Jia, H.X. Gu, W.Q. Jin, N.P. Xu, Acta Mater. 56 (2008) 2687–2698.
[22] H. Zhao, W. Shen, Z. Zhu, X. Li, Z. Wang, J. Power Sources 182 (2008) 503–509.
[23] A.A. Taskin, A.N. Lavrov, Y. Ando, Appl. Phys. Lett. 86 (2005) 091910.
[24] G. Kim, S. Wang, A.J. Jacobson, Z. Yuan, W. Donner, C.L. Chen, L. Reimus, P. Brodersen, C.A. Mims, Appl. Phys. Lett. 88 (2006) 024103.
[25] A.M. Chang, S.J. Skinner, J.A. Kilner, Solid State Ionics 177 (2006) 2009–2011.
[26] A. Tarancon, S.J. Skinner, R.J. Chater, F. Hernandez-Ramirez, J.A. Kilner, J. Mater. Chem. 17 (2007) 3175–3181.
[27] A.A. Taskin, A.N. Lavrov, Y. Ando, Prog. Solid State Chem. 35 (2007) 481–490.
[28] G. Kim, S. Wang, A.J. Jacobson, L. Reimus, P. Brodersen, C.A. Mims, J. Mater. Chem. 17 (2007) 2500–2505.
[29] A. Tarancon, A. Morata, G. Dezanneau, S.J. Skinner, J.A. Kilner, S. Estrade, F. Hernandez-Ramirez, F. Peiro, J.R. Morante, J. Power Sources 174 (2007) 255–263.
[30] K. Zhang, L. Ge, R. Ran, Z.P. Shao, S.M. Liu, Acta Mater. 56 (2008) 4876–4889.
[31] J.H. Kim, Y. Kim, P.A. Connor, J.T.S. Irvine, J. Bae, W. Zhou, J. Power Sources 194 (2009) 704–711.
[32] J.H. Kim, A. Manthiram, J. Electrochem. Soc. 155 (2008) B385–B390.
[33] D.J. Chen, R. Ran, K. Zhang, J. Wang, Z.P. Shao, J. Power Sources 188 (2009) 96–105.
[34] H.T. Gu, H. Chen, L. Gao, L.C. Guo, Electrochim. Acta 54 (2009) 7094–7098.
[35] Q. Zhou, F. Wang, Y. Shen, T. He, J. Power Sources 195 (2010) 2174–2181.
[36] Z.Q. Deng, J.P. Smit, H.J. Niu, G. Evans, M.R. Li, Z.L. Xu, J.B. Claridge, M.J. Rosseinsky, Chem. Mater. 21 (2009) 5154–5162.
[37] M.J. Jorgensen, S. Primdahl, C. Bagger, M. Mogensen, Solid State Ionics 139 (2001) 1–11.
[38] K. Murata, T. Fukui, H. Abe, M. Naito, K. Nogi, J. Power Sources 145 (2005) 257–261.
[39] A.V. Virkar, J. Chen, C.W. Tanner, J.W. Kim, Solid State Ionics 131 (2000) 189–198.
[40] A. Mitterdorfer, L.J. Gauckler, Solid State Ionics 111 (1998) 185–218.
[41] S.B. Adler, J.A. Lane, B.C.H. Steele, J. Electrochem. Soc. 143 (1996) 3554–3564.
[42] S.B. Adler, Solid State Ionics 111 (1998) 125–134.
[43] W. Zhou, B.M. An, R. Ran, Z.P. Shao, J. Electrochem. Soc. 156 (2009) B884–B890.
[44] M.J. Escudero, A. Aguadero, J.A. Alonso, L. Daza, J. Electroanal. Chem. 611 (2007) 107–116.
[45] M.J. Jorgensen, M. Mogensen, J. Electrochem. Soc. 148 (2001) A433–A442.